

FLAME HOLDING DYNAMICS DURING COMBUSTION INSTABILITY IN A SHEAR-COAXIAL INJECTOR COMBUSTOR

Nicolas Guézennec, Timothy Dawson, Patricia Sierra, Suresh Menon

School of Aerospace Engineering
Georgia Institute of Technology
270 Ferst Drive
Atlanta, GA 30332-0150

ABSTRACT

Combustion instability in an experimental high pressure shear coaxial combustor is studied using large-eddy simulation (LES) with a subgrid turbulent mixing closure. In order to match the acoustic mode excitation the entire rig is simulated and it is shown that the simulations reproduce the naturally excited instability in this combustor without any ad hoc adjustments. Two modes in the combustor are shown to contribute to the instability and analysis of the flow-flame interactions shows that a triple flame structure exists in the combustor. This flame structure also undergoes a cyclic motion at the first excited instability frequency. Simulations are shown to capture the changes in the amplitude of the oscillation as the inlet duct length is changed. Results are analyzed to understand the nature of flame holding and its coupling to the acoustic modes in the combustor.

1 Introduction

Thermo-acoustic instabilities, which are organized, oscillatory motions sustained by combustion are detrimental to all operational combustors and are to be avoided in the design phase. They manifest as large amplitude, pressure oscillations and are the result of non-linear coupling between unsteady heat release and the acoustics of the device. Both longitudinal low frequency and transverse high frequency mode instability can occur independently or can coexist depending upon the design and the operating conditions. Instability can excite multiple natural acoustic modes in the combustor and phase lock into specific modes. Fluctuations in fuel flow rate or equivalence ratio, and/or coupling between the boundary conditions and the acoustic-entropy-vortex interactions in the combustor can create an environment that can lead to periodic energy addition in-phase to amplify the naturally occurring pressure oscillations leading to instability (Menon, 2005). Combustion instability can get excited very quickly and can destroy the system. As a result it is very difficult to experimentally sustain and also to predict.

Experimentally, naturally excited instability that can be repeatedly studied and measured have been created only under specialized design constraints. In this study, Large Eddy Simulation (LES) is employed to simulate the experimentally studied Continuous Variable Resonance Chamber (CVRC) test rig based at Purdue University (Yu *et al.*, 2009, 2012). This single element combustor is composed of a coaxial injector and a cylindrical combustion chamber sep-

arated by a dump plane. This type of dump combustor geometry has been extensively used in the past to study combustion instability in ramjets for both premixed and non-premixed combustion using various types of fuel (Poinsot & Veynante, 2001; Menon & Jou, 1991). A feature of such combustors is that under certain operating conditions they exhibited unstable operating conditions related to the excitation of longitudinal acoustic modes in the combustion chamber. The CVRC experiment demonstrates the excitation of such longitudinal modes but also operates (in contrast to many earlier facilities) at very high pressure (1.34 MPa) under oxy-combustion conditions with a high speed stream of oxygen and water vapor injected through the central injector while gaseous methane is injected in the annular duct of the coaxial injector. In the experiments, the length of the oxidizer tube was also varied to change the combustor impedance to study combustion instability under different resonance conditions and it was shown that the amplitude of the pressure oscillations can be changed as a function of the inlet length. Here, simulations are performed for two injector lengths, which represent two known stability conditions: a semi-stable case, and a completely unstable case.

In the past, LES has been successfully employed to study combustion dynamics and instability in various gas-fueled combustion devices, including gas turbines, afterburners and ramjets. In the current study, we employ LES with a subgrid mixing model to investigate combustion dynamics and stability process in the CVRC with a specific goal to investigate the nature of flame holding and coupling with the acoustic modes.

2 Formulation

The Favre-filtered compressible, multi-species LES equations are well known (Menon & Patel, 2006; Masquelet & Menon, 2010) and not repeated here for brevity. In the current approach, the subgrid momentum and energy fluxes are modeled using an eddy viscosity closure for which a transport equation for the subgrid kinetic energy is solved along with the LES equations (Menon & Kim, 1996). The scalar transport and the reaction-diffusion processes at the subgrid scales are modeled using the Linear-Eddy Mixing (LEM) model (Kerstein, 1988). The LEM model is embedded within every LES cell to capture the scalar mixing processes that are not resolved by conventional filtered LES. The processes involved in scalar evolution: molecular diffusion, reaction kinetics, turbulent stirring by subgrid

scale eddies, transport by resolved eddies, volumetric heat release and thermal expansion effects are all explicitly and concurrently included at their respective temporal and spatial scales. The LEM model is a one-dimensional line that is oriented in the direction of the flame normal or maximum scalar gradient with a resolution sufficient to resolve all length scales down to the Kolmogorov scale, η . The subgrid fields are transported across LES cells using a Lagrangian transport model, which ensures mass conservation at the LES level. Finite rate chemistry at the LEM level is modeled using finite-rate kinetics with the laminar rates since the subgrid processes recover the turbulent rates as a part of the simulation. Thus, no closure for the reaction rates or the molecular processes are needed in this approach. More details of the LEMLES formulation and its implemented details are available elsewhere (Menon *et al.*, 1993; Menon & Calhoun, 1996; Menon & Patel, 2006; Menon & Kerstein, 2011) and in the references therein.

The numerical solver is a well established finite-volume, block-structured solver called LESLIE that has been in use for such studies for some time (Menon & Patel, 2006; Genin & Menon, 2010). The solver employs a hybrid method that combines a 3rd order upwind numerical scheme with MUSCL reconstruction alongside an approximate Riemann solver and a 2nd order central scheme for spatial integration with a 2nd order temporal integration scheme. The hybrid method allows overcoming the sensitivity of the central scheme in locations where strong gradients are present by dynamically switching locally to the upwind scheme using a sensor based on pressure and density gradients (Genin & Menon, 2010; Masquelet & Menon, 2010).

Finite rate chemistry is modeled using a 2-step reduced kinetics, 2S_CH4BFER (Franzelli *et al.*, 2010), with five species (CH₄, O₂, CO₂, CO, and H₂O) is chosen for computational efficiency. The original mechanism was designed for CH₄/air flames, and in recent studies modified for use in oxy-methane combustion. Additionally, correction functions were applied to the two pre-exponential factors based on local equivalence ratio in order to avoid an over-prediction of the burning rates and to match the flame speed under high-pressure conditions. Thermally perfect equation of state is employed along with the thermodynamics and transport properties obtained using Cantera.

The central pipe of the coaxial injector supplies the oxidizer mixture (decomposed hydrogen dioxide with water consisting of 0.42% O₂ and 0.58% H₂O per unit mass at $T_{ox} = 1030$ K). The fuel (CH₄ fuel at $T_f = 300$ K) is injected in the annular duct. The test rig operates at a global equivalence ratio of 0.8. Constant-mass NSCBC boundary conditions (Poinso & Lele, 1992) are used at both the in-flows, supplying constant mass flow rates of fuel and oxidizer: $\dot{m}_f = 0.027$ kg/s and $\dot{m}_{ox} = 0.32$ kg/s, respectively. This inflow attempts to mimic the slotted choked inlet of the experiments. The outflow is through a choked nozzle with supersonic exit conditions and is similar to that of the experiment. No-slip, adiabatic walls are implemented everywhere although the injector post-tip and the combustor walls are most likely not adiabatic in the experiment. However, no information on the heat loss is available at this time and this can impact the predicted energy transfer to the oscillations, as noted below.

Figure 1 shows a sketch of the CVRC configuration with the main dimensions (and the relation to the oxidizer duct inner diameter, $D_{Ox} = 2.047$ cm). The experimental rig was designed so different lengths of the central oxidizer

duct of the injector could be tested and results for different inlet duct length have been reported in the past (Yu *et al.*, 2009, 2012). In the current study, we focus on two reported cases that differ only in the length of the oxidizer inlet length but have markedly different dynamics: a semi-stable case for an inlet length $L_{Ox} = 9$ cm and fully unstable case for $L_{Ox} = 12$ cm.

A multi block-structured grid (1.7 million grid points) is used for the simulations with the grid clustered in the regions of high shear and in the early part of the combustor. Earlier studies were carried out to ensure that with such a resolution the shear layer region is well resolved with approximately 6 grid points, which is considered sufficient for the current LES strategy. The LEM resolution is determined by estimating the subgrid Reynolds number (using the local grid size and the subgrid turbulence intensity) at all the LES cells. The largest Re determines the resolution needed (Menon & Kerstein, 2011) and in this study we employ 12 LEM cells in each LES cell. In regions of high turbulence and where flame is seen to exist this resolution implies that all scales down to 0.4η is resolved. Based on past studies this resolution is considered adequate.

Simulations are carried out for approximately $20 \tau^*$, where τ^* is the estimated flow-through time, calculated here to be 2 ms. Analysis is carried out using data after removing the initial transient startup field. As shown below, the instability quickly gets excited and simulation is carried out long enough to confirm that the limit cycle is sustained.

3 Results and Discussion

The experiments showed that the length of the oxygen tube can affect the combustor stability and the magnitude of the excited pressure oscillation. We first discuss briefly the flow features in both time-averaged and instantaneous sense, and then focus on the instability signature, acoustic mode analysis and the nature of flame holding. Comparison with data is carried out wherever possible. We discuss both the cases together in the following sections.

3.1 Flow Field Analysis

Figure 2 shows the time averaged axial velocity and temperature fields for both cases. Figure 2a shows the large corner recirculation zone (CRZ) created downstream of the dump plane. The size of this CRZ is very similar for both cases. The $U=0$ m/s isoline (top, in black) delimits the location of the CRZ, the reattachment point is located at an axial coordinate $x = 3.55D_{Ox}$ in both cases. As discussed later, this recirculation region is crucial to keep the flame ignited and to sustain the instability.

The mean temperature fields are shown in Fig. 2b. The flame length (represented by the $T = 2000$ K isoline) is $5D_{Ox}$ for the 9 cm case and around $4.77D_{Ox}$ for the 12 cm case. The difference in the length of the flame can be related to the location of the triple point structure and its evolution with time, as will be discussed below. It can be seen that the flame is rather long and appears to be approximately anchored at the step corner. The anchoring location can be seen also in the instantaneous fields. For example, Fig. 3 shows typical instantaneous temperature field for both cases. Due to the recess and the high strain rate in the immediate vicinity of the injector lip, the flame cannot stabilize along the stoichiometric mixture fraction isoline as is typical of diffusion flames. Instead, the flame attaches at the step corner, where the reactants have become partially

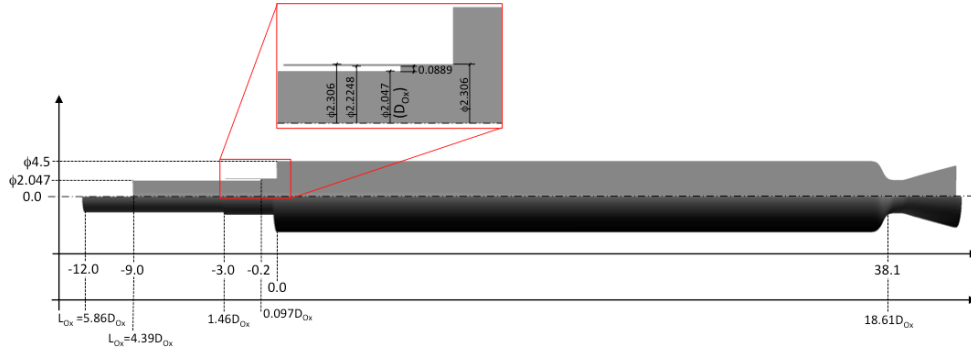


Figure 1: Overview of the CVRC. All dimensions are in cm. The injector region and the two different inlet lengths are shown.

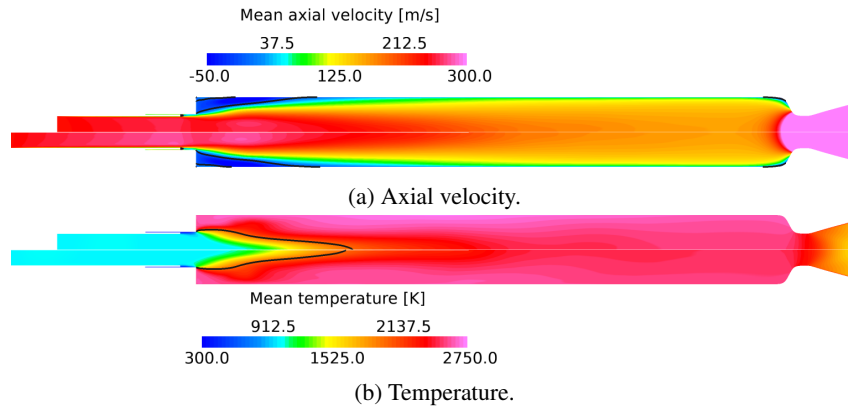


Figure 2: Time-averaged fields. (a) Mean axial velocity ($U = 0$ m/s isoline in black), (b) Mean temperature ($T = 2000$ K isoline in black). Top half of each figure: $L_{Ox} = 9$ cm case; bottom half: $L_{Ox} = 12$ cm case.

premixed and hot products are brought close by the CRZ shown in Fig. 2a. A closer examination (to be further noted below) suggests that the anchoring location moves slightly upstream into the inlet for the 12 cm case whereas, for the 9 cm case it is clearly anchored at the corner. How this anchoring location contributes to the oscillation magnitude is not fully understood but is under study.

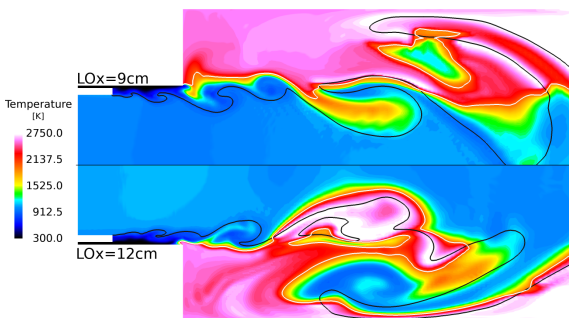


Figure 3: Typical instantaneous temperature field showing the flame anchoring point at the step corner. Upper part: $L_{Ox} = 9$ cm case. Lower part: $L_{Ox} = 12$ cm case. $T = 2000$ K isoline is in black and the stoichiometric mixture fraction $z_{stoich} = 0.095$ isoline is in white.

Although the rich premixed flame is attached at the step corner the remaining fuel-air mixture is consumed further downstream. The resulting triple flame structure (in 3D this is an iso-surface of triple points) with a weak diffusion flame occurring downstream at the location where the rich

premixed and a weaker lean premixed flame intersect. Due to pressure oscillations, the location of the triple flame is not fixed, rather, it propagates from the step corner to approximately $2x/D_{Ox}$ downstream and then returns to the corner at a frequency very close to the first longitudinal mode of the combustor. These features are shown in the instantaneous figures: Fig. 4 where snapshots of the flame (via heat release) and the location of the triple point (as solid points) in a cycle is shown. Also shown is the flame index in the bottom half and it can be seen that the flame is partially premixed with anchoring controlled by the rich premixed flame. The cyclic motion is similar for both inlet cases and therefore, only one case is shown. Further discussion on the triple point motion is given in the later sections.

3.2 Pressure and Acoustic Mode Analysis

Figure 5 shows the signature of the pressure fluctuation, normalized by the mean pressure, \bar{p} , as $\Delta p/\bar{p} = (p - \bar{p})/\bar{p}$ for both cases at an axial location $18D_{Ox}$ downstream of the dump plane. The experimental data, which is available here is also shown. The time is normalized by the first longitudinal mode time scale defined as $t^* = (t - t_0) * F1$, where t_0 is an arbitrary starting time, and F1 is the first longitudinal mode. Although the overall signature is very similar to the experiment, simulation predicts larger peak-to-peak oscillations for both cases. More studies with isothermal wall conditions (i.e., with heat loss) and more detailed kinetics are needed to assess the sensitivity of the predictions to the conditions and modeling approximations.

Table 1 lists the experimental and predicted frequencies of the first three longitudinal modes of the chamber, obtained from the Fourier transform of the pressure fluctua-

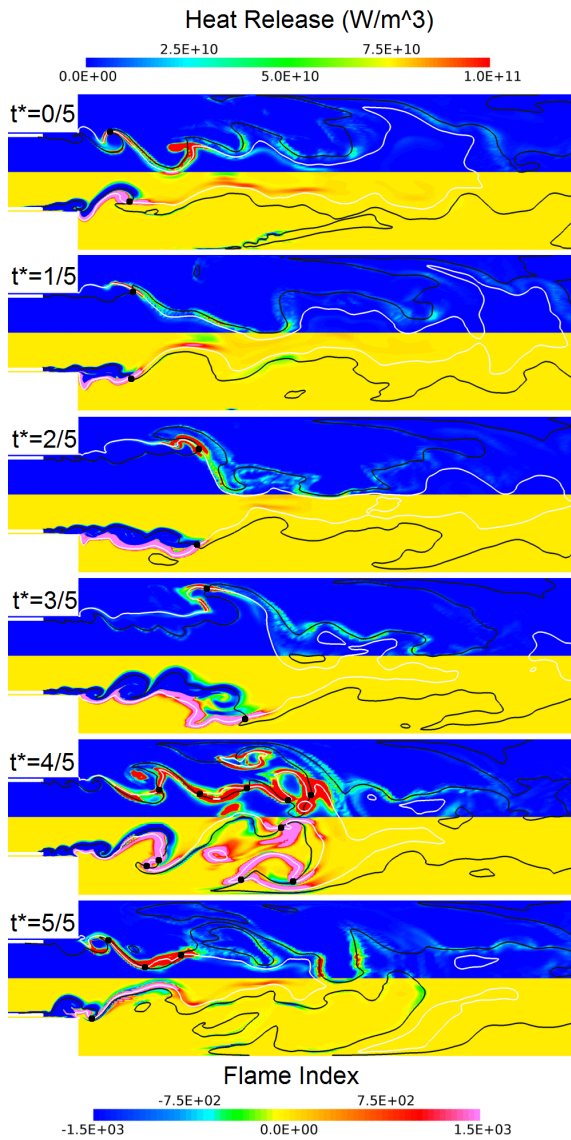


Figure 4: Cyclic motion of the triple flame structure during an oscillation period for $L_{Ox} = 9$ cm. Heat release is in the top half and flame-index is in the bottom half with the triple point(s) shown as solid point(s). Note that the upper and lower halves are the actual halves of a central slice of the combustor and are deliberately shown to highlight the asymmetry in the flow field and the 3D nature of the triple point motion.

tions shown in Fig. 5. As with the amplitude the first mode frequency for both $L_{Ox} = 9$ cm and $L_{Ox} = 12$ cm cases is over predicted by approximately 20%. However, there is much better agreement for the second and third modes. It is interesting to note that as in the experiment, LES also predicts approximately the same frequencies for the modes for both inlet cases. This is expected since these are combustor modes and the dimensions are unchanged.

The amplitude and phase for the first and second modes are calculated along the centerline for the two cases as shown in Fig. 6. The reference point is taken at the dump plane ($x = 0.0$). $L_{Ox} = 9$ cm case shows a pressure node $11.2D_{Ox}$ downstream of the dump plane for the first mode. The second mode shows two nodes located at $x = 3.4D_{Ox}$ and $x = 13.7D_{Ox}$, respectively. The $L_{Ox} = 12$ cm case has

Case	F1 (Hz)	F2 (Hz)	F3 (Hz)
9cm Exp.	1380	2700	3880
9cm Sim.	1690	2720	3440
12cm Exp.	1390	2780	4170
12cm Sim.	1640	3180	4830

Table 1: Frequencies for the first three modes

the pressure node for the first mode at $x = 10.7D_{Ox}$, while the nodes of the second mode are located at $x = 4.4D_{Ox}$ and $x = 14.2D_{Ox}$. So although there are some differences both injector length cases have pressure nodes in the combustor at approximately the same locations. It can also be determined with simple estimated that the first three modes correspond to half, third, and quarter-wave (third mode, not shown here) standing modes in the combustor. On the other hand, analysis shows that there is a traveling wave in the inlet and no nodes exist in the inlet. Additionally, the amplitude of the wave is significantly lower for the $L_{Ox} = 9$ cm case, corresponding to the smaller peak-to-peak amplitude of the pressure oscillations (Fig. 5). This is consistent with the experimental observations.

3.3 Flame Analysis

The stabilization process of the flame is quite complex and cyclic in nature. As discussed in section 3.1, the flame is attached at the step corner instead of the injector lip, the attachment point typically seen in shear coaxial injector configurations. Analysis shows that the strain rate is very high in the shear layer and exceeds the extinction value. Thus, from the injector lip onwards the injected reactants get premixed but ignition is delayed till the recirculation of hot product ignite the partially premixed mixture and sustain the reaction.

Further analysis shows that this partial premixing and ignition downstream results in a complex flame structure and a cyclic process. The anchoring rich premixed flame is soon followed by a triple flame structure. It can be seen that there is diffusion flames along the stoichiometric mixture fraction ($z_{stoic} = 0.095$), while the premixed flames follow the $T = 2000$ K isoline. At the location where the weak diffusion flame intersects the point between the lean and rich premixed flames merge, a triple point can be defined.

In 3D there is actually a triple point surface that is not stationary but moves in a cyclic manner. The motion of this surface can be quantified as a set of radial and axial coordinates, $R(\theta, t)$ and $X(\theta, t)$ in each azimuthal plane. These coordinates can be further reduced by averaging over azimuthal slices to obtain an average instantaneous position of the triple point as shown in Fig. 7. The frequency of cyclic motion of this surface is very close to the frequency of the first mode calculated from the pressure fluctuations for both cases (1700 Hz for the $L_{Ox} = 9$ cm case and 1610 Hz for the $L_{Ox} = 12$ cm case).

Figures 8a and 8b show the triple point locations (in a cross-section) as a scatter of locations colored by discretizing the cyclic time period t^* into five sub periods and allocating a color to each of five equal divisions. There are three notable features shown in these plots: First, the anchor point

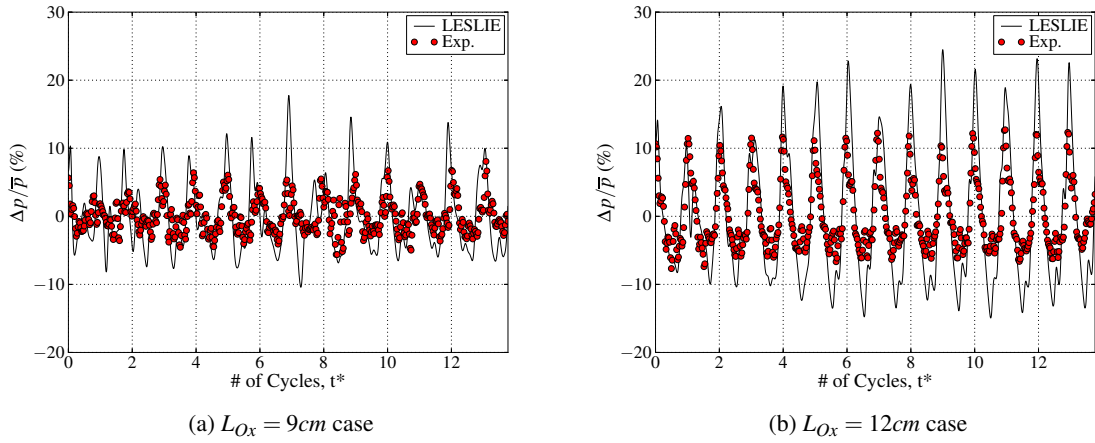


Figure 5: Comparison of experimental and numerical pressure fluctuations $\Delta p/\bar{p}$ for (a) $L_{Ox} = 9\text{ cm}$ and (b) $L_{Ox} = 12\text{ cm}$.

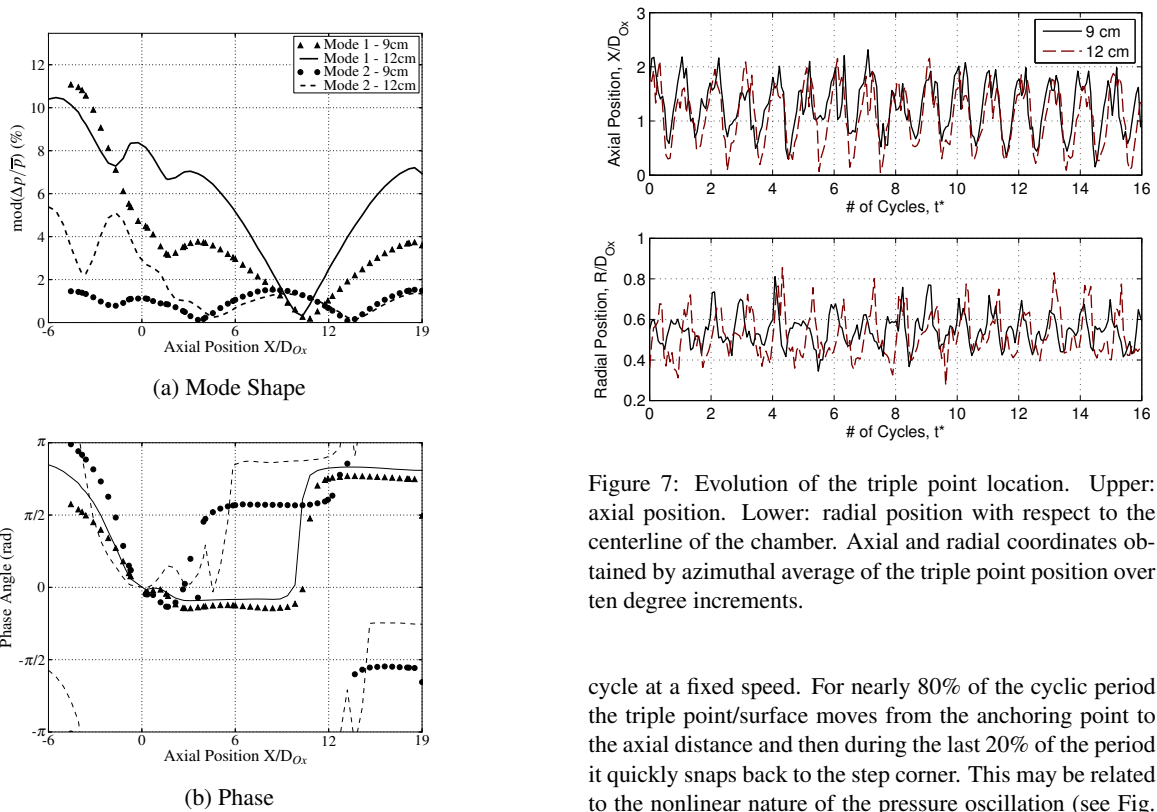


Figure 6: First and second mode shapes (a) and phase (b) as a function of x/D_{Ox} . Note $x/D_{Ox} = 0$ indicates the dump plane. The pressure node for the first mode is at $x/D_{Ox} = 11$, while the two nodes for the second mode appear at $x/D_{Ox} = 4$ and 14 , respectively. There are no pressure nodes in the inlet duct for both cases.

of the $L_{Ox} = 9\text{ cm}$ case is located directly on the step corner at $X/D_{Ox} = 0$ and $R/D_{Ox} = 0.56$, while the $L_{Ox} = 12\text{ cm}$ case anchors slightly within the recess at $X/D_{Ox} = -0.25$ and $R/D_{Ox} = 0.5$. The axial difference of the anchor point exactly correlates with the aforementioned flame length difference. Second, both cases cover a similar area, reaching a maximum radial extension of $R/D_{Ox} = 1$ at $X/D_{Ox} = 1 - 2$ and axial of $X/D_{Ox} = 2.5$ at $R/D_{Ox} = 0.56$. Finally, the triple point motion although cyclic is not traveling in this

Figure 7: Evolution of the triple point location. Upper: axial position. Lower: radial position with respect to the centerline of the chamber. Axial and radial coordinates obtained by azimuthal average of the triple point position over ten degree increments.

cycle at a fixed speed. For nearly 80% of the cyclic period the triple point/surface moves from the anchoring point to the axial distance and then during the last 20% of the period it quickly snaps back to the step corner. This may be related to the nonlinear nature of the pressure oscillation (see Fig. 5, which shows that the positive fluctuation level is much higher than the negative one. Further analysis of this nonlinear process is underway and will be reported soon.

4 Conclusion

LES of combustion instability in a high pressure combustor is carried out with a goal to understand flame holding mechanism under different operating conditions. It is shown that naturally excited pressure oscillations seen in the experiments are also captured in the simulations without any ad hoc model adjustments. Furthermore the effect of changing the inlet oxidizer length is also qualitatively captured as a reduction in the pressure oscillation amplitude with a decrease in the inlet length, consistent with experimental observations. However, the predicted amplitudes are higher in the simulation that may be due to the adiabatic wall conditions and reduced kinetics employed for these

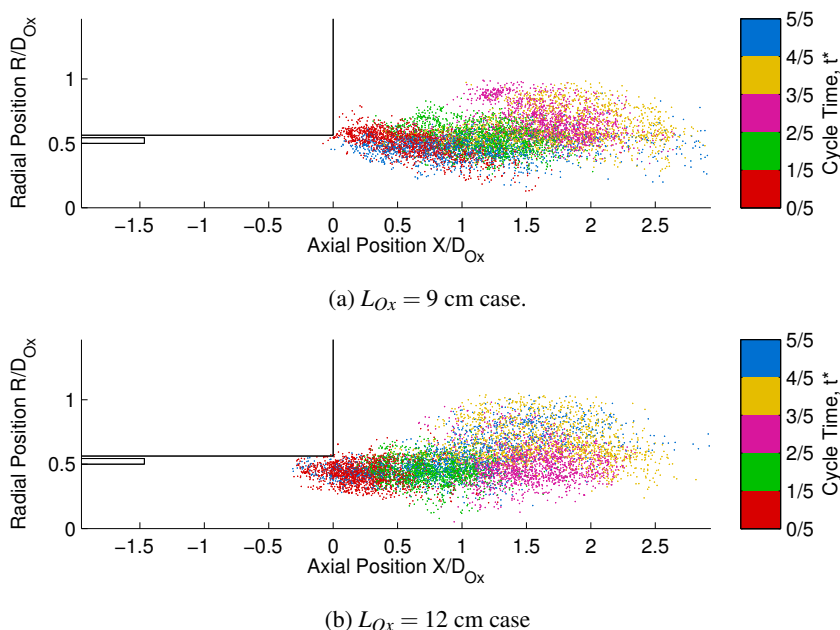


Figure 8: Scatterplot showing the instantaneous location of the triple point. Points are colored by the corresponding division of the oscillation cycle. (a) $L_{Ox} = 9$ cm case, (b) $L_{Ox} = 12$ cm case.

studies. Results show that although the fuel and oxidizer are injected separately, the high strain in the mixing layer results in premixing without ignition, and a rich premixed flame is anchored at the downstream step corner. Subsequent mixing results in a triple flame structure that oscillates between the step corner and the end of the recirculation zone. Future studies will revisit some of these observations with isothermal walls and more detailed kinetics.

Acknowledgements

This work is sponsored in part by Air Force Office of Scientific Research and NASA Glenn Research Center. Simulations were conducted at the DOD High Performance Computing Centers at the Air Force Research Laboratory, WPAFB and the Engineering Research and Development Center, MS. The authors also acknowledge the data provided by Purdue University (Prof. W. Anderson and Dr. T. Feldman) for comparison.

REFERENCES

Franzelli, B., Riber, E., Sanjos'e, M. & Poinso, T. 2010 A two-step chemical scheme for kerosene-air premixed flames. *Combustion and Flame* **157** (7), 1364–1373.

Genin, F. & Menon, S. 2010 Studies of shock/turbulent shear layer interaction using large-eddy simulation. *Computer and Fluids* **39**, 800–819.

Kerstein, A. R. 1988 A linear eddy model of turbulent scalar transport and mixing. *Combust. Sci. Tech.* **60**, 391.

Masquelet, M. & Menon, S. 2010 Large eddy simulation of flame-turbulence interactions in a shear coaxial injector. *J. Prop. Power* **26** (5), 924–935.

Menon, S. 2005 Acoustic-vortex-flame interactions in gas turbine combustors. In *Combustion Instabilities in Gas Turbine Engines: Operational Experience, Fundamental Mechanisms, and Modeling* (ed. Lieuwen T. & Yang V.), vol. 210, pp. 277–314. AIAA.

Menon, S. & Calhoon, W. 1996 Subgrid mixing and molecular transport modeling for large-eddy simulations of turbulent reacting flows. *Proceedings of the Combustion Institute* **26**, 59–66.

Menon, S. & Jou, W.-H. 1991 Large-eddy simulations of combustion instability in an axisymmetric ramjet combustor. *Combustion Science and Technology* **75**, 53–72.

Menon, S. & Kerstein, A. R. 2011 The linear eddy model (LEM). In *Turbulent Combustion Modeling* (ed. T. Echekki & E. Mastorakos), vol. 95, pp. 203–230. Springer.

Menon, S. & Kim, W.W. 1996 High Reynolds number flow simulations using the localized dynamic subgrid-scale model. In *34th Aerospace Sciences Meeting and Exhibit*, AIAA 1996-0425.

Menon, S., McMurthy, P. A. & Kerstein, A. R. 1993 A linear eddy mixing model for LES of turbulent combustion. In *Large-Eddy Simulations of Complex Engineering and Geophysical Flows* (ed. B. Galperin & S.A. Orzag), pp. 287–314. Cambridge University Press.

Menon, S. & Patel, N. 2006 Subgrid modeling for simulation of spray combustion in large-scale combustors. *AIAA Journal* **44** (4), 709–723.

Poinso, T. & Veynante, D. 2001 *Theoretical and Numerical Combustion*. Edwards, Inc.

Poinso, T. J. & Lele, S. K. 1992 Boundary conditions for direct simulations of compressible viscous flows. *Journal of Computational Physics* **101**, 104–129.

Yu, Y. C., O'Hara, Sisco, J. C. & Anderson, W. E. 2009 Experimental study of high-frequency combustion instability in a continuously variable resonance combustor (CVRC). In *47th AIAA Aerospace Sciences Meeting including The New Horizons Forum and Aerospace Exposition*, AIAA Paper 2009-234.

Yu, Y. C., Sisco, J. C., Rosen, S., Madhav, A. & Anderson, W. E. 2012 Spontaneous longitudinal combustion instability in a continuously-variable resonance combustor. *J. Prop. Power* **28**, 876–887.